Journal of Manufacturing Processes 68 (2021) 1683–1693

Contents lists available at ScienceDirect

Journal of Manufacturing Processes

journal homepage: www.elsevier.com/locate/manpro

Failure behavior in electrically-assisted mechanical clinching joints

Abozar Barimani-Varandi [a,*], Abdolhossein Jalali Aghchai [a], Francesco Lambiase [b]

[a] Faculty of Mechanical Engineering, K. N. Toosi University of Technology, 470, Mirdamad Ave. West, Tehran, Iran
[b] Department of Industrial and Information Engineering and Economics, University of L'Aquila, Via G. Gronchi 18, Zona Industriale di Pile, 67100 L'Aquila, Italy

ARTICLE INFO

Keywords:
Joining
Electro-plastic effect
Fracture criteria

ABSTRACT

The failure behavior of AA6061-T6/DP590 clinched joints was investigated using an integrated 2-step FE model. The effectiveness of the electro-plastic effect on the formability and the material flow was studied on aluminum to high-strength steel hybrid clinched joints. An electrical-thermo-mechanical FE model was developed to predict the failure behavior during the tensile shear testing of the joints. Different fracture criteria were applied including Brozzo, normalized Cockroft-Latham, and Rice-Tracey. A new method is proposed to calibrate the abovementioned criteria based on the experimentally determined fracture displacement. The results indicated that the clinched joints made by electrically-assisted mechanical clinching were 46% stronger than those made by conventional mechanical clinching. This was due to increased formability provided by the electro-plastic effect. The numerical model involving the Brozzo fracture criterion showed the highest accuracy. Indeed, the athermal effect of the electro-plasticity led to a hybrid neck fracture mode.

1. Introduction

Lightweight thin-walled structures made in hybrid aluminum alloy to high strength steel assemblies are intensively applied in the automotive body-in-white to reduce the non-renewable energy resources and greenhouse gas emissions. These lightweight assemblies are challenging for joining by conventional resistance spot welding (RSW), friction stirs spot welding, and self-piercing riveting (SPR). Joining sheets with dissimilar thicknesses and different properties, e.g. melting point, thermal conductivity, density, Young's modulus, and intermetallic formed compounds can be easily performed by the mechanical clinching (MC) [1–3].

MC process produces joints by producing a mechanical interlock through a severe localized plastic deformation using a simple punch and an anvil. Therefore, the success in joining depends on the sheet's material ductility. Although the mechanical behavior in MC is mainly dictated by the final geometry, the microstructure and the mechanical properties of clinching materials also affect the performance of joints. Indeed, bottom thickness (BD) is a key geometrical parameter particularly to experimentally assess the strength in a non-destructive control. The geometric parameters i.e. neck thickness (t_N), undercut length (t_U), and bottom thickness as shown in Fig. 1, are the main geometrical parameters of a clinched joint [4–6].

Based on the ISO 12996:2013, four failure modes may occur when a clinched joint is failed in a tensile shear testing. The non-adequate geometrical interlocking and small neck thickness may cause the failure of joints in the pull-out (PO) and neck fracture (NF) modes, respectively. Two hybrid failure modes may occur when there is a good balance between the undercut length and neck thickness including hybrid pull-out (HP) and hybrid neck fracture (HN) modes. Lei et al. [7] comprehensively studied the abovementioned failure modes using the tensile shear testing for four types of metal materials (SPCC, DP590, TA1, and AL142). They concluded that the joints that undergone hybrid failure showed excellent load-bearing capacity and energy absorption ability.

Peng et al. [8] reviewed the latest advances of clinching technologies on the development of tools and processes. Many researchers determined the mechanical behavior of the clinched joints. Zhao et al. [9] identified the material parameters using a Rousselier model modified by Guo et al. [10]. They calibrated the criterion through an inverse method comparing the experimental results with the numerical simulations using shear and tensile tests [9]. Lambiase and Di Ilio [11] described the evolution of ductile damage to predict the onset of the fracture during the MC of similar AA6082-T6 sheets, using a 2D axisymmetric FE model. They calibrated the fracture criteria through an inverse technique by fitting the load-stroke predicted curve with experimental data [12].

In electrically-assisted processes, the effect of electrical current on the mechanical behavior of a metal is termed as an electro-plastic effect.

* Corresponding author.
E-mail address: barimani.abozar@email.kntu.ac.ir (A. Barimani-Varandi).

https://doi.org/10.1016/j.jmapro.2021.06.072
Received 9 April 2021; Received in revised form 1 June 2021; Accepted 29 June 2021
Available online 9 July 2021

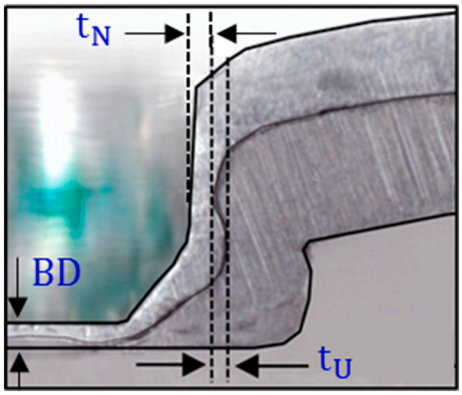

Fig. 1. Main geometric parameters of a clinched joint.

This effect was firstly assessed and reported by Troitskii and Likhtman in 1963 [13]. Significant changes will occur in the material behavior at the threshold current values of the current density [14]. Theories related to the electro-plastic effect are divided into two groups of thermal and athermal effects. Researches in thermal effect discussed thermal softening according to the Joule heating theory at hot condition [15,16]. Zhang et al. [17] firstly introduced a novel resistance spot clinching (RSC) for joining aluminum alloy 5052 sheets, and compared with the RSW joints. Then, they investigated effects of the oxide film on the RSC aluminum sheets [18], effects of local stiffness on the RSC joints [19], and resistance rivet clinching of AA5754/ DQSK sheets [20]. All their tests were done at high-orders values of electrical current values above 8 kA which imposed a hot condition. Comparatively to the RSW joints, their joints consisted of a larger equiaxed zone at the fusion zone, increased joint strength, and superior toughness. However, their method is very challenging for the Al/St materials owing to different melting points and thermal conductivity, the easy formable Fe-Al brittle intermetallic compounds, and the presence of oxide layers for aluminum sheets [1,21]. Besides, Lou et al. [22] proposed a resistance riveting, named rivet-welding, by adopting a 13 kA welding current to improve the robustness and strength of the Al/St joints. They found that the electrical current improved the microstructure of the joint, and 12.1% higher tensile shear strength could obtain compared with the traditional SPR process [22].

On the other hand, Nguyen-Tran et al. reported that, since the athermal effect is a cost-effective and an energy-saving phenomenon that also improves the final quality, most electro-plastic manufacturing processes are often performed at this condition. In which, low values of electrical current values often below 1000 A generate relatively low temperatures within the moderate warm condition [23]. The authors proposed the MC process with the help of an electrically-assisted preheating operation, in which controlling the material flow was achieved by applying a newly defined chamfer ratio to guarantee the strong mechanical interlock [1]. They recently investigated the tensile shear strength for joining low-ductility aluminum to high-strength steel by using electrically-assisted mechanical clinching (EAMC) [21]. Indeed, Lou et al. [24] proposed a new electrically-assisted SPR to reduce the deformation resistance of AA6061-T6/DP780 sheets, by applying a low-orders values of direct current during the process. Comparatively to the traditional SPR joints, their joints increased by 12.5% and 23.3% in tensile shear strength and cross-tension strengths, respectively [24].

The ductile fracture initiates with the growth and coalescence of microscopic voids; this is governed by a large stress triaxiality in a meso-field of plastic strains [25]. According to the complex stress state and the hybrid fracture mechanism in the tensile shear testing of clinched joints, phenomenological ductile fracture including Brozzo [26], normalized Cockroft-Latham [27], and Rice-Tracey [28] were utilized. They are presented in Eqs. (1)–(3) in terms of stress triaxiality (η) as well as normalized Lode angle parameter ($\bar{\theta}$), as the dimensionless ratios derived from the stress invariants.

$$\mathrm{CDVB} = \int_0^{\bar{\varepsilon}_p} \left(\frac{2}{3} + \frac{\eta}{\cos\left(\frac{\pi}{6}(1-\bar{\theta})\right)} \right) \mathrm{d}\bar{\varepsilon}\mathrm{p} \tag{1}$$

$$\mathrm{CDVC-L} = \int_0^{\bar{\varepsilon}_p} \left(\eta + \frac{2\cos\left(\frac{\pi}{6}(1-\bar{\theta})\right)}{3} \right) \mathrm{d}\bar{\varepsilon}\mathrm{p} \tag{2}$$

$$\mathrm{CDVR-T} = \int_0^{\bar{\varepsilon}_p} \exp\left(1.5\,\eta\right) \mathrm{d}\bar{\varepsilon}\mathrm{p} \tag{3}$$

where $\mathrm{CDV_B}$, $\mathrm{CDV_{C\text{-}L}}$, and $\mathrm{CDV_{R\text{-}T}}$ respectively represent the critical damage values for Brozzo, normalized Cockroft-Latham, and Rice-Tracey. The crack initiates at any point in the mesh whenever the damage exceeds the $\mathrm{CVD_i}$.

This paper is aimed at studying the failure behavior of the joints clinched by the electro-plastic effect with the aid of a FE model involving damage fracture criteria, at current value equal to 500 A. A newly proposed method, which is more similar to a tensile test in terms of stress state and loading path, was utilized to predict the failure loads and modes during the tensile shear testing of the clinched joints. The calibration procedure based on the experimentally determined fracture displacement was applied for the first time in a strength evaluation of the MC process to determine the damage value. The cross-section of the fractured joints was investigated to assess the failure mechanism for various processing conditions.

2. Material and methods

2.1. Mechanical properties

Aluminum alloy sheets (AA6061-T6) were clinched to DP590 + Z140 with thicknesses of 1 mm and 1.5 mm, respectively. The aluminum sheet was positioned at the punch side, while the steel sheet was positioned at the die side. The chemical compositions of materials are reported in Table 1. The uniaxial tensile tests based on the ASTM-E8 standard were performed with a constant speed of 1 mm/s at a current density range up to 50 A/mm^2 (Fi. 2).

According to Fig. 2a, at a current density of 40 A/mm^2, significant changes occur in the mechanical behavior of DP590 compared with lower values. Since the behavior is relatively similar up to 30 A/mm^2, the threshold density for steel sheets lies in the density range of 30–40 A/mm^2. Then at 50 A/mm^2, the tensile strength is reduced due to the electro-plastic effect. Indeed, the formability is also increased slightly. On the other hand, for the aluminum sheet, the changes of mechanical behavior are almost small and gradual with increasing density up to 50 A/mm^2. To assess the strength of the clinched joints, quasi-static tensile shear tests (TST) were applied with a constant crosshead speed of 2 mm/min, according to ISO 12996. In Fig. 3 the geometry of the test specimens used in the both uniaxial tensile and tensile shear testing are depicted.

2.2. Experimental setup

An anvil with an initial diameter of 5.6 mm and a depth of 1.3 mm was adopted. Besides, a conical-shaped punch with a diameter of 4.6 mm and a chamfer length of 1.30 mm at the constant angle of 45°, via a surrounding rubber blank holder were used. The universal testing machine model STM-20 by SANTAM was used to perform the clinching tests with tools mounted on the two guided upper and lower shoes with a ram speed of 10 mm/min. The clinching tools were made of warm working hardened steel (DIN 1.2344). The clinching tools with detailed

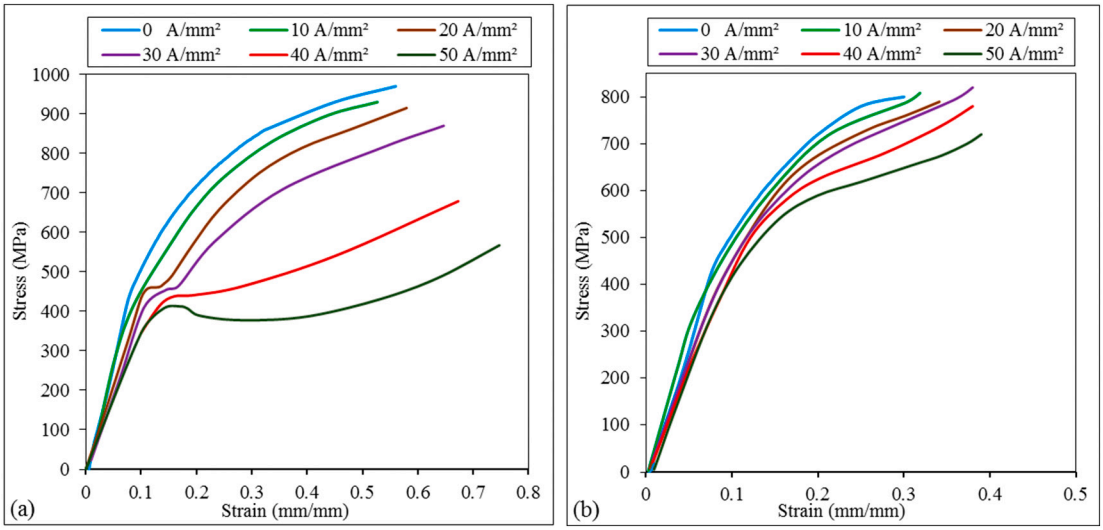

Fig. 2. Stress-strain curves in various values of current density for (a) DP590 and (b) AA6061.

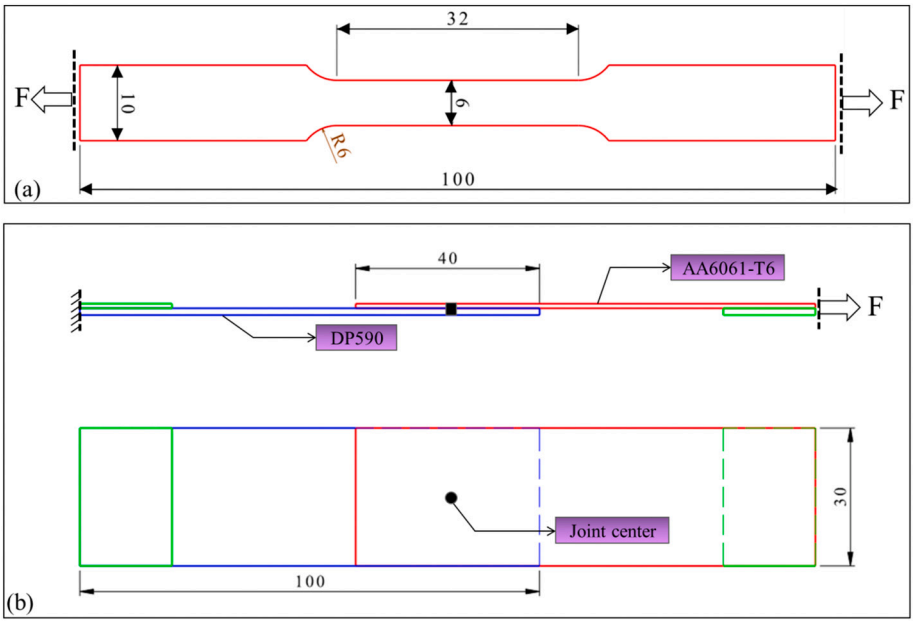

Fig. 3. Geometry of the test specimen used in testing of (a) uniaxial tensile and (b) tensile shear.

dimensions are depicted in Fig. 4. The chamfering punch shown in Fig. 4b increases the punch-anvil cavity volume and consequently can lead to more radial material flow. The easiness of a radial flow prevents an early fracture near the punch corner as well as can promote larger interlocks [1]. Additionally, for electrically-assisted heating the joint region during the clinching process, a fixture was designed which was equipped with an autotransformer flowing by the alternating current. The schematic of the EAMC is depicted in Fig. 5.

The location of the electrodes efficiently enabled the electrical current to flow through the upper (aluminum) sheet through the copper ring, then flowed out from the lower sheet to the pin positioned in the anvil as the other electrode. A current amount of about 500 ± 5 amps was used in all the EAMC experiments for a period of 10 s. This current value was chosen based on the allowed nominal amplitude of the adopted equipment. Also, longer holding times were not involved to prevent possible overheating issues. The sheets were insulated from the setup components using the thin layers of mica film. Two K-type thermocouples were utilized to measure the temperature variation of upper and lower sheets at the joint center. More importantly, the safe range of penetration depth (P), i.e. respectively 3.3–3.6 mm for MC and 2.7–3.2 mm for EAMC, were experimentally determined to guarantee the successfully clinched joints including the absence of neck fracture on the upper sheet, the formation of the interlock, and crack-free bulged bottom of the lower sheet.

2.3. FE simulation

A 3D numerical model for typically quantifying the accurate current density using the ABAQUS software package, as well as an integrated 2-step numerical model for multiphysics simulation by 3D FEM code DEFORM were used. Due to the existence of thermal and also electric fields, the ABAQUS/implicit coupled thermal-electric was applied. The linear element of a type DC3D8E with 8 nodes by both temperature and electric potential degrees of freedom were employed.

To predict the tensile shear strength of EAMC joints, a 2-step numerical model provided by a DEFORM V11 multiple operations interface

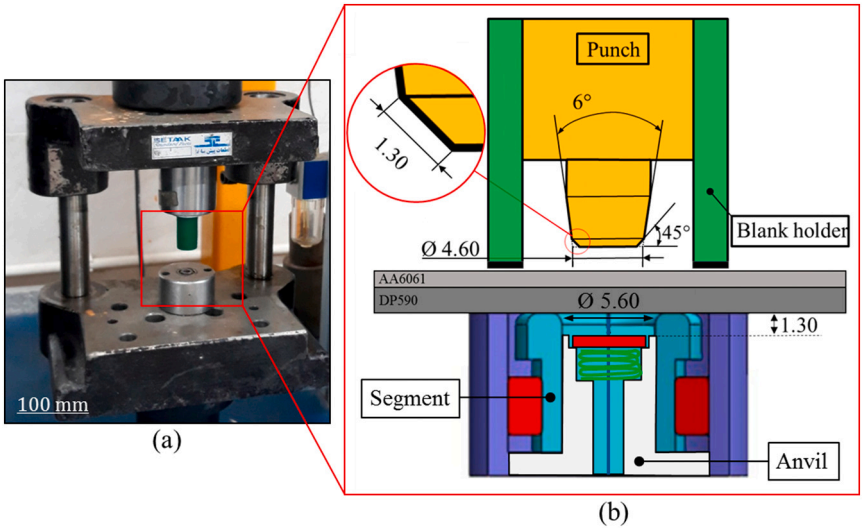

Fig. 4. (a) Clinching process die setup and (b) main dimensions of the tools (mm).

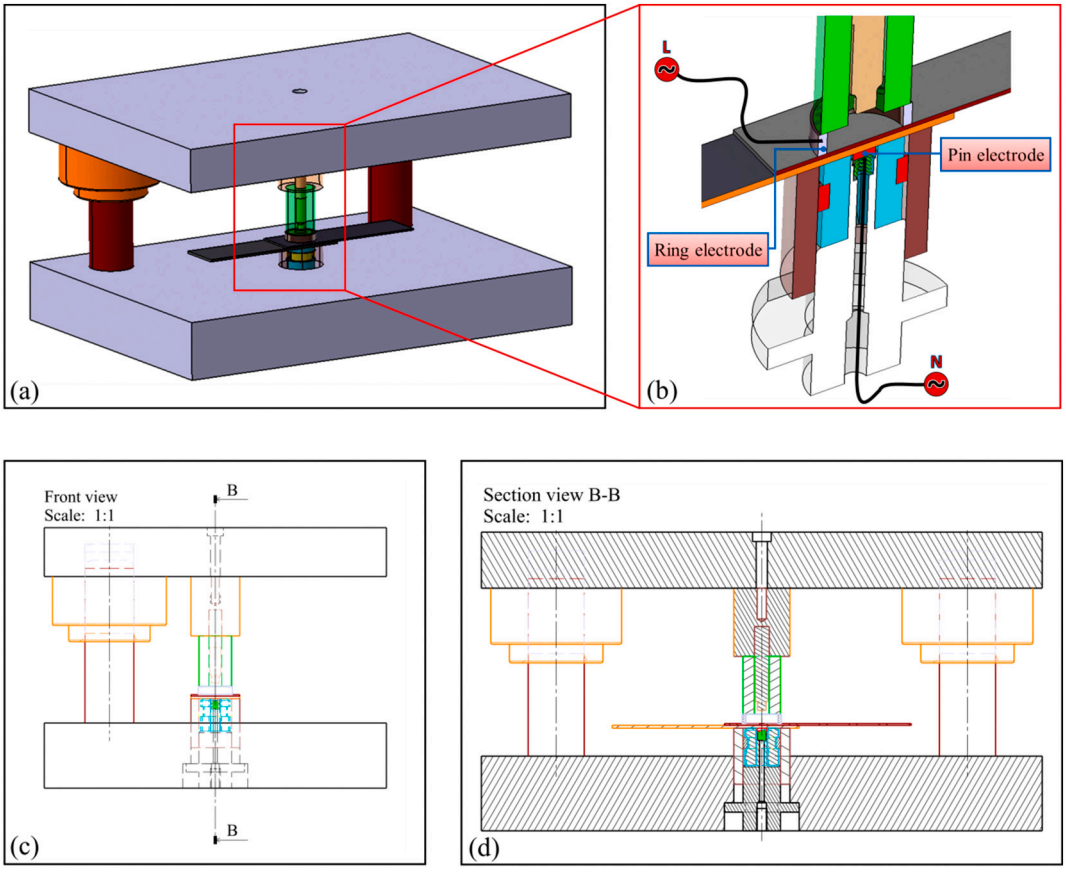

Fig. 5. Schema illustration of the EAMC die: (a) 3D view, (b) 3D section of tools, (c) 2D front view, and (d) section view from a front view.

was utilized. The numerical model involved a coupled electrical, thermal, and mechanical simulation for the EAMC process (step 1) followed by mechanically tensile shear testing of clinched joints (step 2). The electrical parameters were applied as recently reported by the authors [1]. The strain-stress history resulted in step 1 automatically was converted to step 2 by using a multiple operations interface. To assign the material property, strain-stress data obtained from uniaxial tensile tests regarding the current density value was applied. The simulation in step 1 was stopped based on the prescribed stroke. Note that at the end of step 1, the punch was retracted to consider the spring back as well as to cool down the sheets. In step 2, to simulate the TST, the experimentally achieved fracture displacement was applied as a criterion for stopping.

Linear 4-node tetrahedral elements were adopted for discretization. A model with the finer mesh in regions exposed by high plastic strains was used. Conditions of the frictional contact were inserted according to the previous work by the authors [1]. The typical defects induced by clinching, namely neck fracture, absence of interlock, and the cracks in the lower sheet should be prevented. The joints were not affected by

aforesaid defects with the employment of safe P ranges. Thus, ignoring the fracture criteria for the FE model in step 1 will not cause a sensible deviation in predicted results.

3. Results

3.1. Current density distribution

The determination of the current density distribution is a prerequisite to understanding material behavior. Experimental measurements and numerical prediction of the temperature at the top aluminum (ToAl) and the bottom of the steel sheet (BoSt) located at the center of the overlap area are compared in Fig. 6. A non-penetrating punch was applied for easy experimental measurements of the temperature, i.e. just the current with the same processing time was applied. Both the experimental measurements and the numerical prediction indicate that the temperature rise was more marked at the bottom steel side as compared to the upper aluminum side. This was ascribed to the greater electrical resistance of the steel. Besides, Fig. 6 indicates that the numerical model provided an overprediction of the temperature as compared to the experimental measurements with a maximum deviation of 8%. This was ascribed to the loss of heat due to defects in insulation, as well as the heat transfer to the environment.

The current density contour and distribution at 500 A are shown in Fig. 7. Fig. 7 indicates that the numerical predictions may not differ significantly by experimental measurements; as the current density is just affected by the amount of the electric current and the cross-section area [29]. Although the current density for the punch-sided aluminum sheet is lower than that of the steel sheet, according to the magneto-plasticity theory, the electric current flow will facilitate the dislocations motion by creating a magnetic field, reducing flow stress, and improving the material flow, as was assessed by Golovin [30] and Molotskii and Fleurov [31]. On the other hand, it was expected that the higher electrical resistance of steel causes a larger electro-plastic effect than the AA6061 side [32]. The maximum current density is about 45 A/mm^2 for steel sheets at 500 A, which is higher than the threshold current density according to the mechanical behavior of 590DP steel (please refer to Section 2.1). The Joule heating effect was not noticeable due to the slight temperature increase at the steel sheet (relative to the melting point). Thus, the athermal effect of the threshold current density may play a key role to improve mechanical behavior [15]. Besides, although increasing the employment time of the current flow rises the maximum temperature and thus the thermal softening of the Joule heating effect, it would not strongly influence the final results [33]. For the current equal to 500 A, due to generated current density in the range of the DP590 threshold value, the athermal effect of the electro-plasticity promises ongoing results that involve reduced forming force and increased strength because of the promoted grain refinement [21,34].

3.2. Calibration of ductile fracture criteria

The damage parameter, i.e. CDV_i, was determined and validated through a uniaxial tensile test (UTT) and a newly presented method based on the tensile shear testing (TST). The critical damage values obtained for both calibration tests were calculated according to the presented procedure in Fig. 8. The damage criterion was just accounted for the AA6061 punch-sided sheet, whereas it was ignored for the DP590 anvil-sided sheet. Because of that no failure was also observed experimentally on the lower sheet. Indeed, the bulged bottom cracks in the anvil-sided sheet may not affect the static strength in the clinching process, as provided by Coppieters et al. [35]. They observed that these cracks did not have a detrimental effect on the static strength and fatigue life of single shear lap specimens [35]. Besides, the uniaxial tensile test was simulated similarly to the recent works that previously calibrated the uncoupled ductile criteria [36,37].

An integrated 2-step model was developed to calibrate the damage parameter according to the newly proposed calibration test. Here, the sheets joined in FE model step 1 were loaded under tensile shear condition until a displacement that involved the experimental fracture (from the experimental results). The location of the critical elements and the calculated CVD_i are presented in Fig. 9 and Table 2, respectively. Please note that MC tests for damage calibration were performed in such a way as to induce neck fracture in subsequent tensile loading.

Fig. 9 indicates that the critical element for the UTT was located in the center of the gauge length. However, the critical element with the highest effective plastic strain was positioned on the neck region of the upper sheet for TST, i.e. the neck fracture mode could be confirmed. The comparisons summarized in Table 2 indicate that the CVDs values for UTT were higher than those determined by TST. The UTT presents an upper bound for damage initiation. After determination the CVDs, the numerical results for both steps including EAMC and TST were validated using the developed FE model to extract the final results. For this purpose, at first, a well-verified comparison of the cross-sections at $P = 3.2$ mm are shown in Fig. 10. The neck fracture and no interlocking are the main defects of the MC which will fail the joints. So, the sound joints in safe P ranges are not affected by these defects. It shows that ignoring the damage criterion for step 1 may not tangibly affect the final results.

In order to verify the FE model in step 2, the tests experimentally failed at the EAMC process obtained from a fracture initiation, i.e. modes of neck fracture and hybrid neck fracture were simulated using the aforesaid damage criteria, to assess the calibration tests and fracture criteria. The failure load changes are presented in Fig. 11. For each condition in Fig. 11, the experimental results were plotted for five repetitions with black dashed lines. The average (Ave.) trendline for each condition was plotted to accurately compare the results. The numerical results obtained from TST provided more accurate predictions of the trend, maximum force, and displacement with less than 13% deviation. The calibration test which was more similar to the experiment in terms

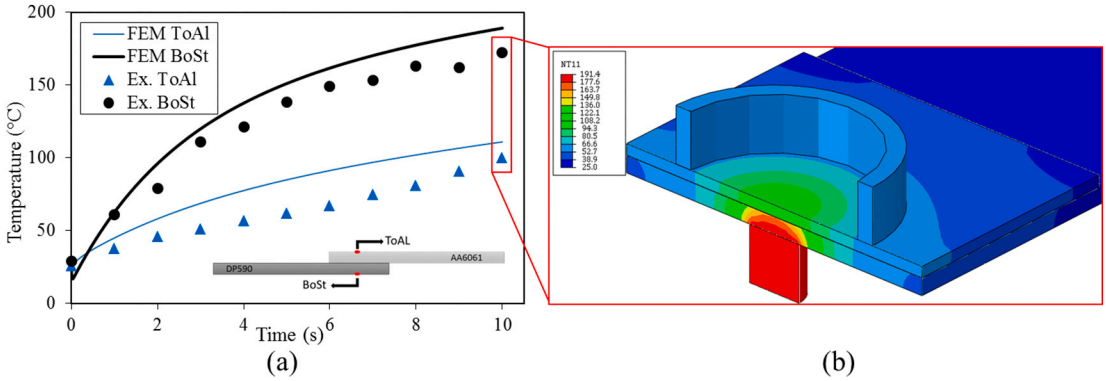

Fig. 6. Comparison of temperature changes at 500 A.

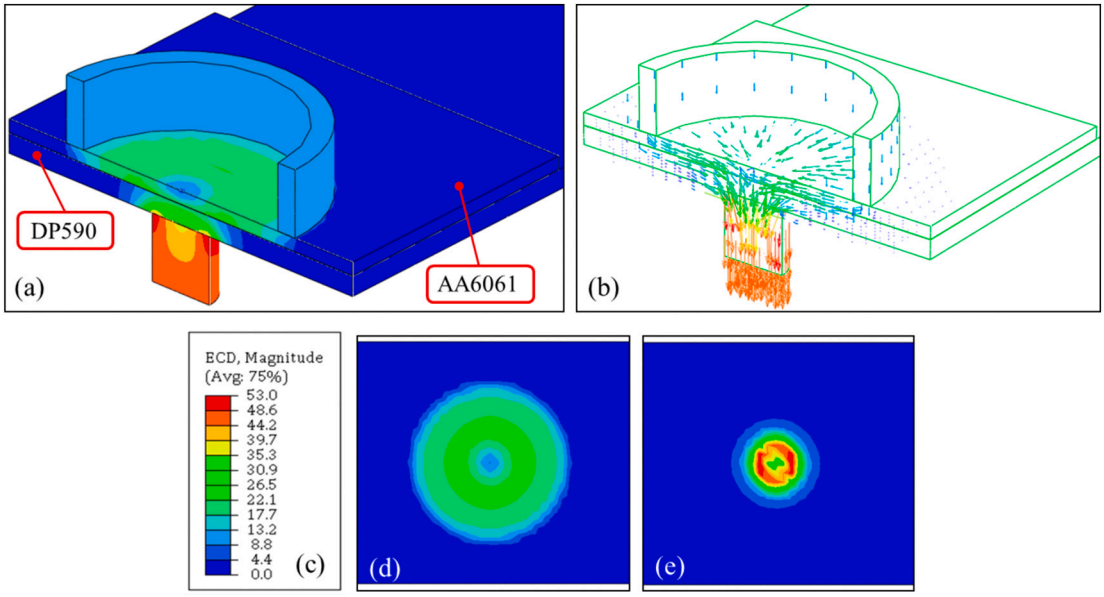

Fig. 7. (a) Current density contour, (b) current flow direction of contour for (c) current density distribution, (d) top view of the upper sheet, and (f) bottom view of the lower sheet.

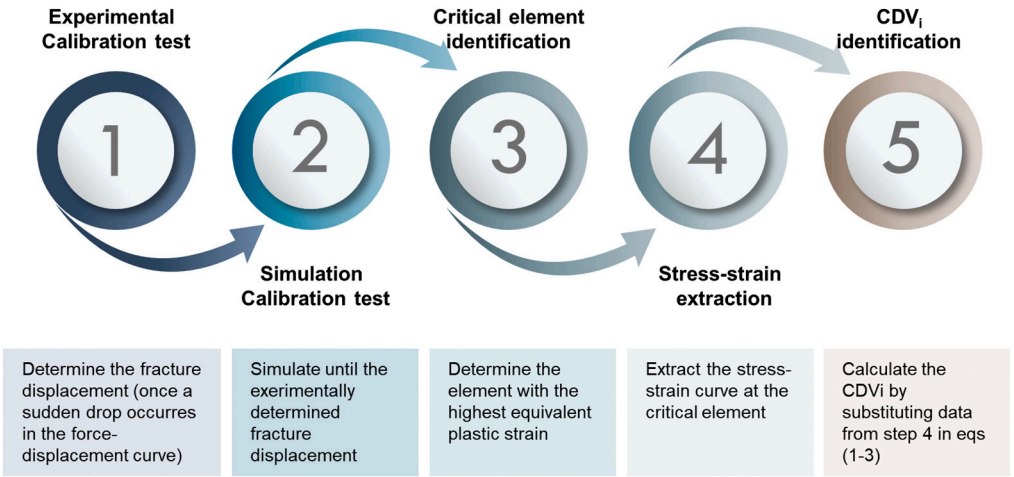

Fig. 8. Stages of the calibration procedure.

of loading and stress state, i.e. TST compared with UTT, provided more accurate predictions of the load-displacement trends. Consequently, the TST was applied to further study ductile fracture criteria in the next section.

3.3. Failure behavior

Fig. 12 depicts the influence of the safe P ranges on key quality geometrical characteristics of the clinched connections t_N and t_U. Thinner necks, as well as larger undercut lengths, were produced for the EAMC process. The electro-plastic effect improved the formability and led to a larger interlock by facilitating the radial material flow. The average slope of the undercut increase was more than the average decrease rate of the neck thickness, respectively +25% and −7%. Referring to Fig. 6b, the arrangement of the electrodes on both sides of the sheets could localize the current flow on the joint center. Therefore, according to the electromigration effect which was reported by Pan et al. [38] and the electron wind theory by Ruszkiewicz et al. [15], facilitating the movement of the electrons toward the joint center can result in a higher momentum transfer which leads to the increased ductility, reduced forming force, and reduced spring back. As a result, the increased formality in the EAMC condition could produce a large interlock. However, providing enough material to radial flow was accompanied by a slight reduction in the neck thickness.

In Fig. 13, the predicted peak loads based on the applied fracture criteria were compared with the experimental results. Exponential trendlines were fitted for changes of maximum failure load, which was predicted with applied fracture criteria. All three criteria overestimated the loads since the Brozzo criterion had the least deviation with an average of less than 10%. Ignoring the material anisotropy and damage criteria in step 1 as well as aggregation of the errors during two steps can justify this deviation. Similar to the Brozzo criterion, the models with a dependence of a damage accumulation on both η and $\bar{\theta}$ produced more accurate results. It was found by Wierzbicki et al. where they introduced a new experimental technique to characterize fracture behavior of metals under bi-axial and tri-axial state of stress condition [39]. Referring to Fig. 12, the numerical thicker undercuts, as well as ignored damage phenomena in step 1, led to the enhancement of the load-bearing capacity. As a result, it could be expected to have a failure load overestimation as shown in Fig. 13. The utilized fracture criteria in

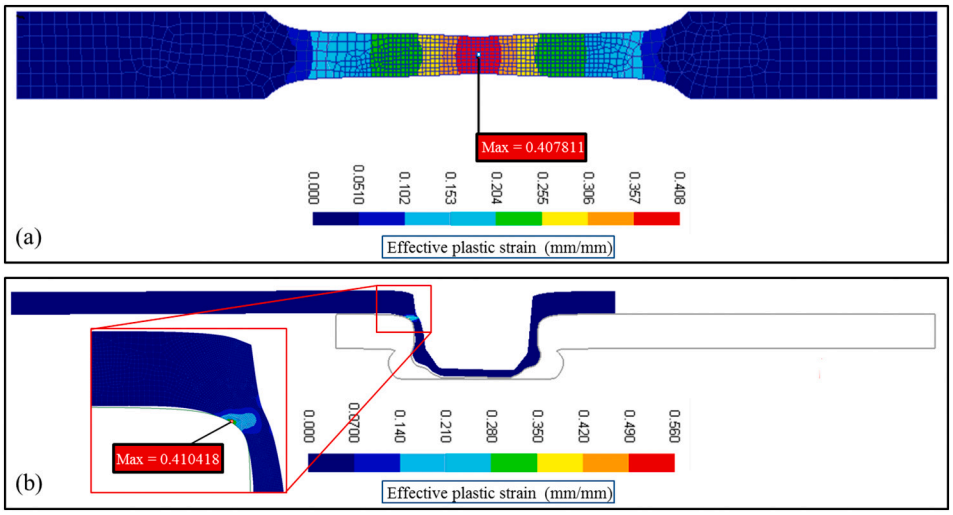

Fig. 9. Location of the critical elements for EAMC (a) UTT on AA6061 and (b) TST on Al/St clinched joint.

Table 2
Critical damage values of AA6061 for three ductile fracture criteria.

Criteria	Calibration test	MC	EAMC
Brozzo	UTT	0.386	0.546
	TST	0.328	0.442
C-L	UTT	0.335	0.474
	TST	0261	0.388
R-T	UTT	0.290	0.407
	TST	0.240	0.301

step 2 predicted three regions in terms of failure mode for both MC and EAMC processes. In the following, experimental fracture modes were studied using numerical results to track the failure mechanism.

The joints experimentally failed by pull-out mode due to an insufficient geometrical interlocking (at low values of the penetration depth). This mode was characterized by the complete separation of the upper sheet from the anvil-sided sheet as illustrated in Fig. 14a–c. The FE model in Fig. 14c can determine the failure initiation during pull-out mode originated from a tensile loading. The pull-out mode started by rotating the upper sheet around the interlock region A and then led to a full separation due to the weak undercut. Larger undercuts were capable of bearing much more deformation before the complete separation of the upper sheet. Indeed, when higher strokes were used, the strength of the interlock exceeded the strength of the upper neck. Thus, when the shear load reached the strength of the localized neck, the cracks propagated rapidly in the peripheral direction until it caused a ring shape fracture of the upper neck (Fig. 14d–f). The high-magnification area in Fig. 14f shows the failure initiation of the neck fracture mode. The horizontal direction of the crack propagation path in Figs. 14e and 14f show the dominant exerted shear loading which came with slight deformation.

At the upper bound of punch strokes, the hybrid fracture modes occurred. For the tensile shear testing of conventional MC tests, the failure mode was similar to the pull-out mode where the upper sheet was completely ripped off from the hook, as shown in Fig. 15a. Fig. 15c depicts that the upper sheet began to exit from the hook by rotating around the neck region; thus, the pull-out failure mechanism was first activated. Subsequently, during the separation of the upper sheet from the lower sheet, due to the large induced-deformation around the rotation center B, the upper sheet fractured from the neck region which can be interpreted from Fig. 15b. This fracture occurred due to the major

Table 1
Chemical composition of the material (wt%).

	Ti	Zn	Cr	Mg	Mn	Cu	C	Si	P	S	Fe	Ni	Al	N	Sn
AA6061	0.11	0.20	0.18	0.93	0.09	0.20	–	0.72	–	–	0.58	–	Balance	–	–
DP590	–	–	0.02	–	1.01	<0.02	0.09	0.28	0.01	0.01	Balance	<0.02	0.04	0.01	0.01

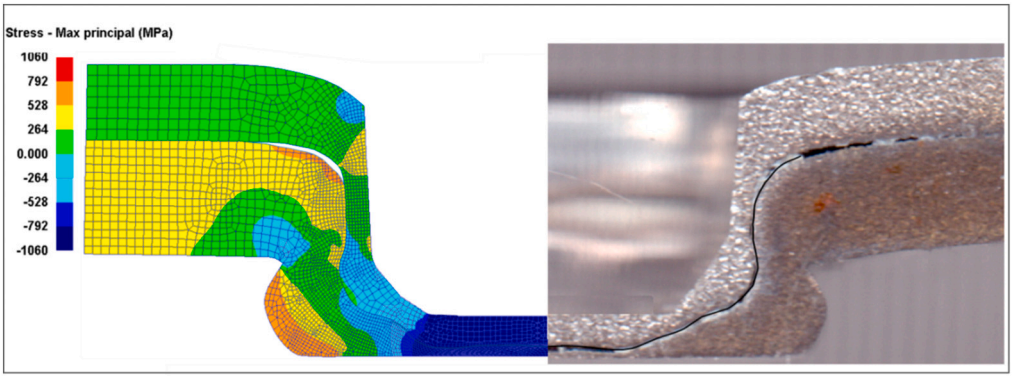

Fig. 10. Numerical and experimental cross-sections for EAMC.

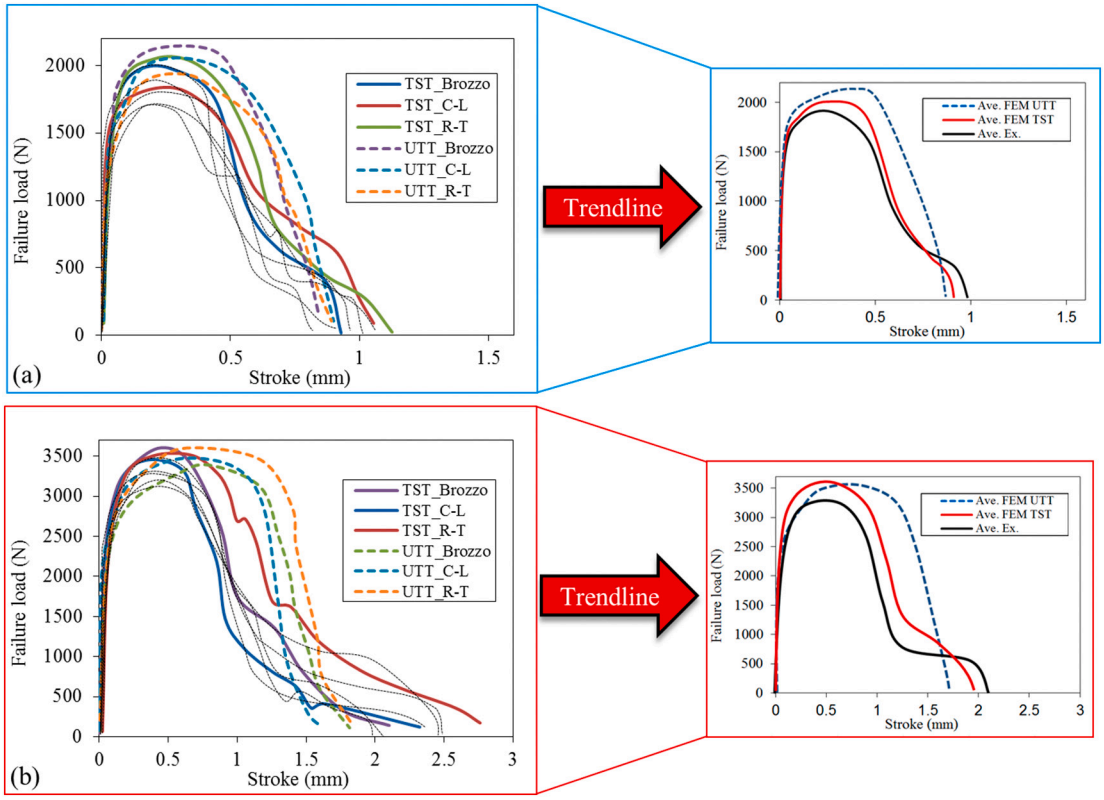

Fig. 11. Failure load variations for EAMC with modes of (a) NF and (b) HN.

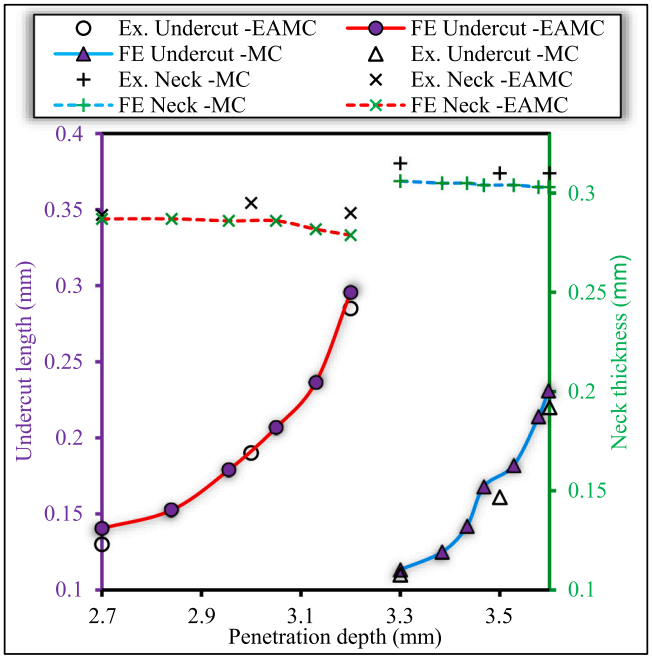

Fig. 12. Changes of t_U and t_N in terms of penetration depth.

contact force exerted by the strong interlock. However, a weak undercut prevented arising of the neck fracture in individual pull-out mode (Fig. 15a–c). In Figs. 15b and 15c, the crack propagation direction shows the mixed impact of the shear and tensile loading. The load-bearing capacity of the joint was degraded due to the propagated crack. Accordingly, a full separation was generated accompanied by a partial propagation of the neck crack. The deformation rate after the occurring fracture was not large.

The clinched joints that failed in a hybrid neck fracture mode at EAMC, involved large plastic deformation. The hybrid pull-out mode was replaced by a hybrid neck fracture mode. This led to 46% of strength enhancement. In hybrid neck fracture mode, the fracture neck propagated peripherally with much more deformation as compared to a pure neck fracture mode. This was due to the increased formability obtained from the electro-plastic effect. The failure order in this mode is reversed relative to the other hybrid mode, in which the primary neck fracture was followed with incomplete button separation of the lower pit, i.e. region C in Fig. 15e. The results reported in Fig. 15f indicate that the neck fracture was the first activated failure mechanism. Besides, the deformation of region C originated from the tensile loading verifies the high plastic deformation induced by this failure mode.

4. Discussion

The mechanical clinching process represents a suitable process for joining hybrid multi-materials assemblies. However, clinching low-ductility aluminum alloys with high-strength steel alloys can be severely affected by the poor formability of the materials. The electro-plastic effect obtained from EAMC can improve the material flow as well as enhancing the ductility. Previous researches reported various potential advantages of the electro-plastic effect at low current values within the warm condition, from an athermal effect point of view, i.e. environmentally friendly, simplicity, high efficiency, and improved mechanical strength.

In this study, EAMC has been applied to join the AA6061-T6/DP590 sheets. The clinching process depends on the ductility of the sheets which determines the joint geometry and therefore the final strength. To evaluate the mechanical behavior of the joint, failure modes and loads should be considered. Besides, failure displacement is also important to assess the energy absorption by a joint. The capability of predicting the failure mode and how it occurs should be tracked incrementally

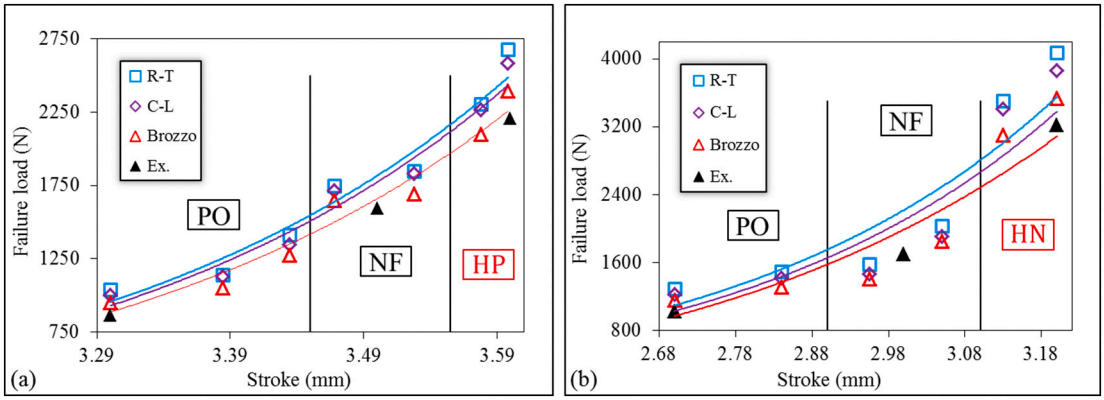

Fig. 13. Maximum failure loads variation and fitted trendlines with numbered failure regions in (a) MC and (b) EAMC.

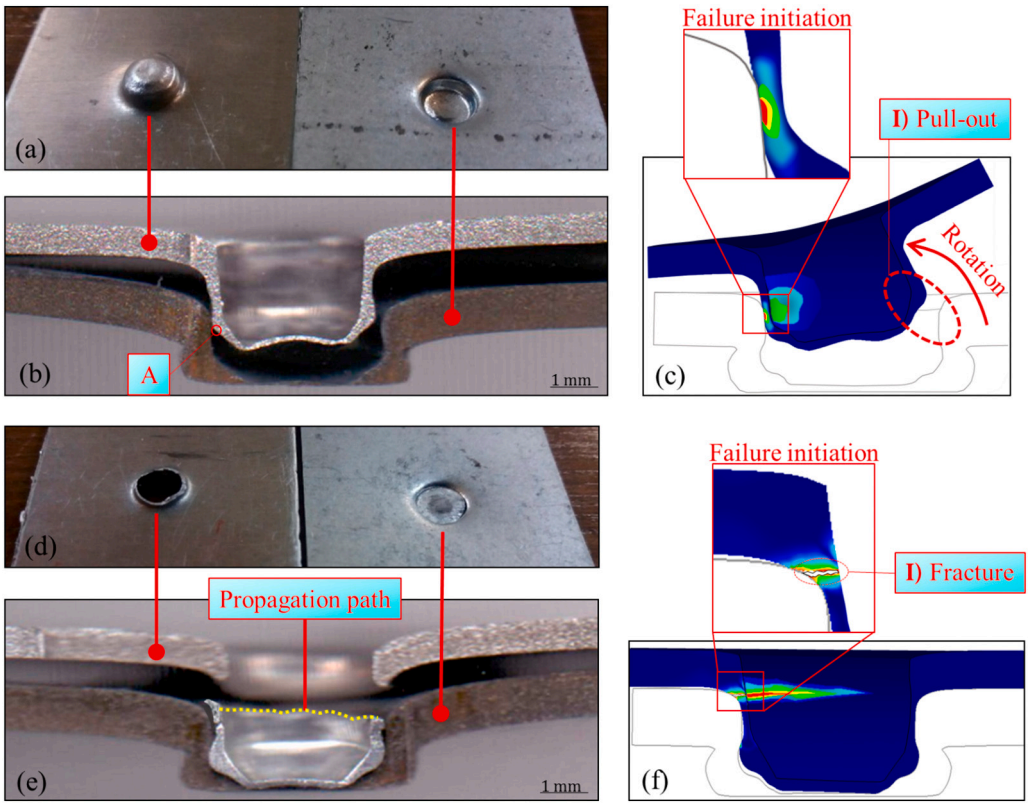

Fig. 14. Pull-out failure mode (a–c) and neck fracture mode (d–f).

represents a pivotal aspect to create high-strength clinched joints. This can be performed using numerical models involving fracture and damage evolution models. The 2-step FE simulation model was developed and validated in the present study to meet this demand. This model also involves the material behavior and its dependency on the current density. Crossing the results from the tensile shear testing, material property, and failure behavior, four failure modes were observed:

1. Joints with an insufficient undercut failed by a pull-out mode;
2. Joints with a thin neck relative to interlock length failed by a neck fracture mode;
3. Joints with an interlock length slightly smaller than the neck thickness failed by a hybrid pull-out mode;
4. Joints with an interlock length a little larger than the neck thickness failed by a hybrid neck fracture mode.

The developed approach enabled to select accurately the optimal current density distribution, explore the failure initiation and its propagation path, failure mode, and failure load-displacement changes. This was achieved by predicting the influence of the current density-dependent material property, as well as by involving a damage criterion and developing a new calibration procedure. The operating range of the current density was initially determined with the aid of the FE model to define the material property. The newly proposed calibration method that was more similar to the TST in terms of loading and stress state represented a reliable tool to predict the failure behavior. Besides, the calibration procedure, which was based on the experimentally determined fracture displacement, improved the model accuracy also when predicting the experimental measurement of the load-displacement trends during the joining. The integrated 2-step FEM multiphysics model provided significant improvements. Indeed, the strain-stress history resulted in the EAMC was converted to step 2 to tensile shear

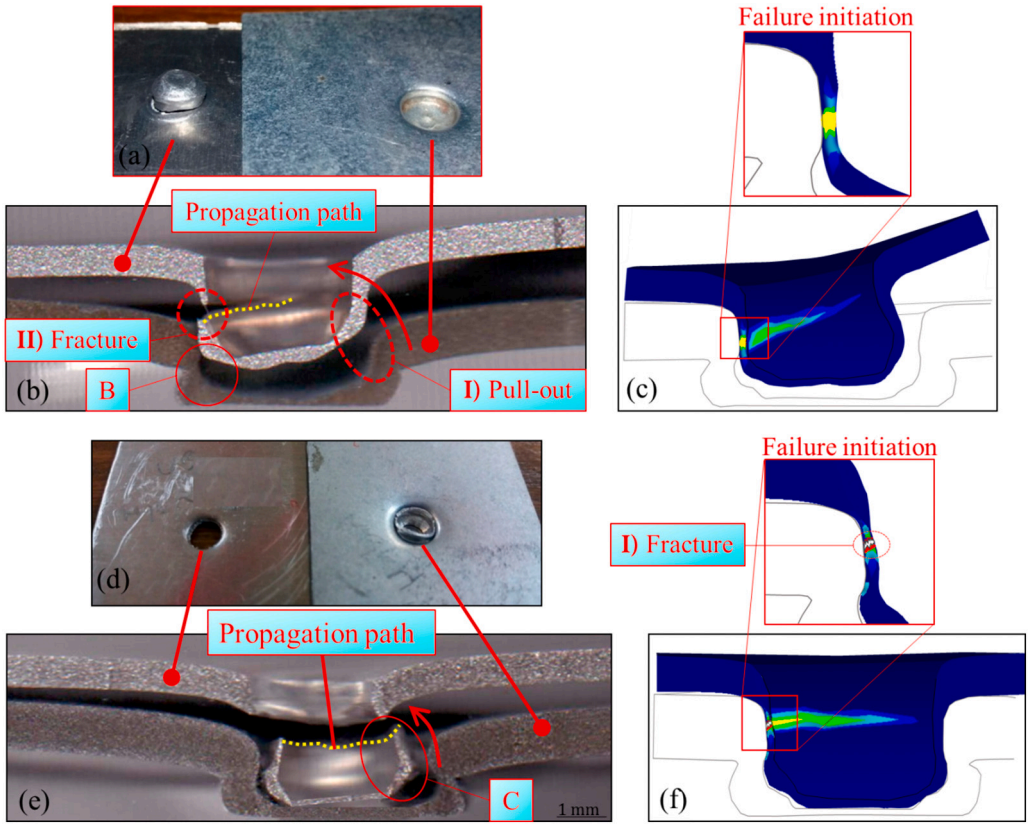

Fig. 15. (a–c) Hybrid pull-out failure mode and (d–f) hybrid neck fracture mode.

testing. Also, various uncoupled fracture criteria were available. The ability to automatic remeshing should be also noted which prevents severe distortion of the elements and therefore the early divergence.

The results indicated that the joint with the highest strength failed by the hybrid neck fracture mode. This was characterized by high values of the penetration depth at the electrically-assisted condition. This strength was 46% higher than the conventional process obtained from the athermal effect of the electro-plasticity. This is far enough above the AWS recommended requirement for the strength of Al/St resistance spot-welded joints [1].

The material property was identified at the constant speed, while the speed affects the strain rate, particularly at elevated temperatures. The relatively low generated temperature can be a justification for this simplification. Nevertheless, it can be one of the causes of the error of the model about 10%. Thus, further efforts can focus on identifying the material property regarding both current density and strain rate-dependency.

5. Conclusion

A 2-step integrated electrical-thermo-mechanical model was developed to simulate the failure mechanism of the Al/St clinched joints under tensile shear testing. The mechanical clinching experiments were performed with the aid of the electro-plastic effect. Three uncoupled fracture criteria were compared and calibrated using the uniaxial tensile tests as well as a newly proposed method. The experimental fracture displacement was chosen as a calibration criterion. The main results are reported as follows:

1. The electro-plastic effect in EAMC showed a good performance to efficiently improve the material formability and consequently the possibility to use the clinching process on low-ductility aluminum alloys to high-strength steels;
2. The developed integrated model demonstrated that the failure evolution can be predicted with a reasonable accuracy in terms of the initiation moment and propagation path;
3. the numerical results indicated that the adoption of a current of 500 A can form a large interlock. Also, this inhibited the fracture developing at the punch corner region for the upper AA6061 sheet owing to the induced formability (magneto-plasticity). Besides, according to the athermal effect of electro-plasticity, less forming force and high strength were achieved due to the generated current density around the threshold value of the DP590 sheet;
4. the tensile shear testing calibration test provided better performances relative to the uniaxial tensile method in terms of capability to predict the failure load changes;
5. the Brozzo criterion with the dependence of the damage accumulation on both stress triaxiality and normalized Lode angle parameter could acceptably depict the maximum failure load with an average error rate of about 10% by timely capturing the failure initiation;
6. occurring hybrid neck fracture mode in EAMC, which is characterized by the large plastic deformation at medium temperature ranges, confirmed the efficiency of the athermal effect of the electro-plasticity in joining the low-ductility-to-high-strength sheets. This mode resulted in a 46% enhancement in maximum failure load compared to the highest failure load achieved in MC.

Declaration of competing interest

The authors declare that they have no known competing financial interests or personal relationships that could have appeared to influence the work reported in this paper.

References

[1] Barimani-Varandi A, Aghchai AJ. Electrically-assisted mechanical clinching of AA6061-T6 aluminum to galvanized DP590 steel: effect of geometrical features on material flow and mechanical strength. Mechanics & Industry 2020;21(5):529.
[2] Lambiase F, Grossi V, Paoletti A. Friction Stir Joining of CFRP laminates with amorphous polymers: influence of processing speeds. J Manuf Process 2020;55:186–97.
[3] Mucha J. The analysis of lock forming mechanism in the clinching joint. Mater Des 2011;32(10):4943–54.
[4] Coppieters S, Lava P, Hecke R Van, Cooreman S, Sol H, Houtte P Van, et al. Numerical and experimental study of the multi-axial quasi-static strength of clinched connections. Int J Mater Form 2013;6(4):437–51.
[5] Mucha J, Witkowski W. The clinching joints strength analysis in the aspects of changes in the forming technology and load conditions. Thin-Walled Struct 2014;82:55–66.
[6] Lee C-J, Kim B-M, Kang B-S, Song W-J, Ko D-C. Improvement of joinability in a hole clinching process with aluminum alloy and carbon fiber reinforced plastic using a spring die. Compos Struct 2017;173:58–69.
[7] Lei L, He X, Yu T, Xing B. Failure modes of mechanical clinching in metal sheet materials. Thin-Walled Struct 2019;144:106281.
[8] Peng H, Chen C, Zhang H, Ran X. Recent development of improved clinching process. Int J Adv Manuf Technol 2020:1–31.
[9] Zhao S, Xu F, Guo J, Han X. Experimental and numerical research for the failure behavior of the clinched joint using modified Rousselier model. J Mater Process Technol 2014;214(10):2134–45.
[10] Guo J, Zhao S, Murakami R-i, Zang S. Experimental and numerical investigation for ductile fracture of Al-alloy 5052 using modified Rousselier model. Comput Mater Sci 2013;71:115–23.
[11] Lambiase F, Ilio A Di. Damage analysis in mechanical clinching: experimental and numerical study. J Mater Process Technol 2016;230:109–20.
[12] Hambli R, Reszka M. Fracture criteria identification using an inverse technique method and blanking experiment. Int J Mech Sci 2002;44(7):1349–61.
[13] Troitskii O, Likhtman V. The Anisotropy of the Action of Electron and Gamma Radiation on the Deformation of Zinc Single Crystals in the Brittle State. Soviet Physics Doklady; 1963. p. 91.
[14] Conrad H. Electroplasticity in metals and ceramics. Mater Sci Eng A 2000;287(2):276–87.
[15] Ruszkiewicz BJ, Grimm T, Ragai I, Mears L, Roth JT. A review of electrically-assisted manufacturing with emphasis on modeling and understanding of the electroplastic effect. J Manuf Sci Eng 2017;139(11).
[16] D'Urso G. Thermo-mechanical characterization of friction stir spot welded AA6060 sheets: experimental and FEM analysis. J Manuf Process 2015;17:108–19.
[17] Zhang Y, Shan H, Li Y, Guo J, Luo Z, Ma CY. Joining aluminum alloy 5052 sheets via novel hybrid resistance spot clinching process. Mater Des 2017;118:36–43.
[18] Zhang Y, Shan H, Li Y, Zhao CF, Luo Z, Guo J, et al. Effects of the oxide film on the spot joining of aluminum alloy sheets: a comparative study between resistance spot welding and resistance spot clinching. Int J Adv Manuf Technol 2017;92(9):4231–40.
[19] Zhang Y, Zhang X, Guo J, Manladan SM, Luo Z, Li Y. Effects of local stiffness on the spot joints mechanical properties: comparative study between resistance spot welding and resistance spot clinching joints. J Manuf Process 2019;39:93–101.
[20] Zhang Y, Wang C, Shan H, Li Y, Luo Z. High-toughness joining of aluminum alloy 5754 and DQSK steel using hybrid clinching–welding process. J Mater Process Technol 2018;259:33–44.
[21] Barimani-Varandi A, Aghchai A Jalali. Enhancement of the tensile shear strength for joining low-ductility aluminium to high-strength steel by using Electrically-Assisted Mechanical Clinching (EAMC). In: Proceedings of the Institution of Mechanical Engineers. Part B: Journal of Engineering Manufacture; 2021.
[22] Lou M, Li Y, Wang Y, Wang B, Lai X. Influence of resistance heating on self-piercing riveted dissimilar joints of AA6061-T6 and galvanized DP590. J Mater Process Technol 2014;214(10):2119–26.
[23] Nguyen-Tran H-D, Oh H-S, Hong S-T, Han HN, Cao J, Ahn S-H, et al. A review of electrically-assisted manufacturing. Int J Pr Eng Man-GT 2015;2(4):365–76.
[24] Lou M, Li Y, Li Y, Chen G. Behavior and quality evaluation of electroplastic self-piercing riveting of aluminum alloy and advanced high strength steel. J Manuf Sci Eng 2013;135(1).
[25] Lemaitre J, Desmorat R. Ductile, creep, fatigue and brittle failures. In: Engineering Damage Mechanics; 2005.
[26] Brozzo P, Deluca B, Rendina R. A new method for the prediction of formability limits in metal sheets. Proc 7th Biennal Conf IDDR 1972;1:18–25.
[27] Oh S, Chen C, Kobayashi S. Ductile Fracture in Axisymmetric Extrusion and Drawing—Part 2: Workability in Extrusion and Drawing. 1979.
[28] Rice JR, Tracey DM. On the ductile enlargement of voids in triaxial stress fields*. J Mech Phys Solids 1969;17(3):201–17.
[29] Chen K, Liu X, Ni J. Electrically assisted friction stir spot welding of aluminum alloy to advanced high strength steel. In: ASME 2017 12th International Manufacturing Science and Engineering Conference Collocated With the JSME/ASME 2017 6th International Conference on Materials and Processing. American Society of Mechanical Engineers Digital Collection; 2017.
[30] Golovin YI. Magnetoplastic effects in solids. Phys Solid State 2004;46(5):789–824.
[31] Molotskii M, Fleurov V. Magnetic effects in electroplasticity of metals. Phys Rev B 1995;52(22):15829.
[32] Mai J, Peng L, Lin Z, Lai X. Experimental study of electrical resistivity and flow stress of stainless steel 316L in electroplastic deformation. Mater Sci Eng A 2011;528(10–11):3539–44.
[33] Perkins TA, Kronenberger TJ, Roth JT. Metallic Forging Using Electrical Flow as an Alternative to Warm/Hot Working. 2007.
[34] Lu Y, Qu T, Zeng P, Lei L, Fang G, Sun J. The influence of electroplastic rolling on the mechanical deformation and phase evolution of Bi-2223/Ag tapes. J Mater Sci 2010;45(13):3514–9.
[35] Coppieters S, Zhang H, Xu F, Vandermeiren N, Breda A, Debruyne D. Process-induced bottom defects in clinch forming: simulation and effect on the structural integrity of single shear lap specimens. Mater Des 2017;130:336–48.
[36] Talebi-Ghadikolaee H, Naeini HM, Mirnia MJ, Mirzai MA, Gorji H, Alexandrov S. Fracture analysis on U-bending of AA6061 aluminum alloy sheet using phenomenological ductile fracture criteria. Thin-Walled Struct 2020;148:106566.
[37] Talebi-Ghadikolaee H, Naeini HM, Mirnia MJ, Mirzai MA, Alexandrov S, Zeinali MS. Modeling of ductile damage evolution in roll forming of U-channel sections. J Mater Process Technol 2020;283:116690.
[38] Pan R, Wang Q, Sun D, He P. Effects of electric field on interfacial microstructure and shear strength of diffusion bonded α-Al_2O_3/Ti joints. J Eur Ceram Soc 2015;35(1):219–26.
[39] Wierzbicki T, Bao Y, Bai Y. A new experimental technique for constructing a fracture envelope of metals under multi-axial loading. In: Proceedings of the 2005 SEM Annual Conference and Exposition on Experimental and Applied Mechanics; 2005. p. 1295–303. Portland USA.